Inorganic Chemistry

Article

pubs.acs.org/IC

Anosovite-Type V_3O_5: A New Binary Oxide of Vanadium

D. Weber,[†] C. Wessel,[‡] C. Reimann,[§] C. Schwickert,[⊥] A. Müller,[†] T. Ressler,[†] R. Pöttgen,[⊥] T. Bredow,[§] R. Dronskowski,[‡] and M. Lerch*

[†]Institut für Chemie, TU Berlin, Straße des 17. Juni 135, D-10623 Berlin

[‡]Institut für Anorganische Chemie, RWTH Aachen University, Landoltweg 1, D-52056 Aachen

[§]Institut für Physikalische und Theoretische Chemie, Universität Bonn, Wegelerstraße 12, D-53115 Bonn

[⊥]Institut für Anorganische und Analytische Chemie, Universität Münster, Corrensstraße 30, D-48149 Münster

ABSTRACT: The reaction of either $V_2F_6{\cdot}4H_2O$ or a mixture of 60 wt % $VF_2{\cdot}4H_2O$ and 40 wt % $VF_3{\cdot}3H_2O$ with a water-saturated gaseous mixture of 15−20 vol % hydrogen in argon leads to the formation of a new polymorph of V_3O_5 crystallizing in the orthorhombic anosovite-type structure. Quantum-chemical calculations show that the anosovite-type structure is about 15 kJ/mol less stable than the corresponding monoclinic Magnéli phase. In addition, there are no imaginary modes in the phonon density of states, supporting the classification of the anosovite-type phase as a metastable V_3O_5 polymorph. Susceptibility measurements down to 3 K reveal no hint for magnetic ordering.

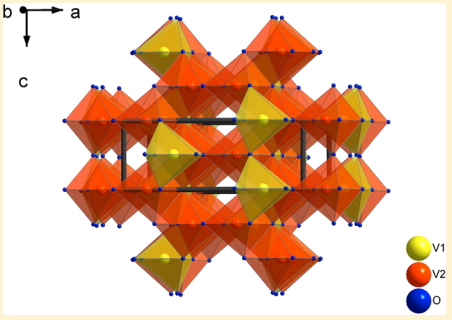

INTRODUCTION

In the last few decades, great interest has been attracted by the various potential applications of vanadium oxide-based materials, arising from the physical and chemical properties of these compounds. They are used in various areas, for example, as catalysts,[1,2] chemical sensors,[3] cathode materials for high-density lithium batteries,[4] and in other electronic and optical devices.[5] As a matter of fact, binary vanadium oxides, in particular, exhibit a wide range of unique characteristics and have been the subject of numerous investigations. One example is V_3O_5, the first member of the homologous series V_nO_{2n-1} (n = 3−9), known as Magnéli phases.[6,7] The existence of this vanadium oxide was first reported by Andersson in 1954 on the basis of X-ray data. He determined a monoclinic unit cell that contains four formula units V_3O_5.[8] Andersson suggested the space group to be $P2/c$ which, in a subsequent contribution by Horiuchi et al., was revised to be $P2_1/n$.[9] The interesting physical and structural properties of this compound have been described in detail in a number of publications relating to the variable valence of vanadium with partly filled 3d orbitals.[10−15] At 428 K, V_3O_5 undergoes a first-order transition of semiconductor-metal-type,[16,17] which is accompanied by a change in symmetry from $P2/c$ or $P2_1/n$ to $I2/c$. At ambient pressure, V_3O_5 shows antiferromagnetic ordering below T_N = 75 K and paramagnetic behavior above T_N.[14,15,18] The crystal structures of LT- and HT-V_3O_5 can both be described as a hexagonal close packing of oxygen atoms where 3/5 of the octahedral sites are occupied. More information on the structural details is given by Åsbrink.[19]

The preparation of new binary vanadium oxides is still a challenge in solid state chemistry. Recently, we reported the synthesis of a new metastable polymorph of vanadium sesquioxide that crystallizes in the bixbyite-type structure.[20] In this contribution, we now describe the synthesis, crystal structure, and high-temperature behavior of a new polymorph of V_3O_5 that can be obtained by an analogous route. The local structure and magnetic properties are investigated by experimental techniques, while complementary quantum-chemical calculations prove the (meta)stability of the new phase.

EXPERIMENTAL SECTION

All reactions were carried out in a conventional tube furnace equipped with a corundum tube with an inner diameter of 50 mm. The flow rate of the reaction gas (15−20 vol % H_2 in Ar, gas stream piped through a water-filled washing flask) was regulated with a parallel arrangement of two mass flow controllers (Brooks Instrument) and has been optimized to 5 L h^{-1}. A total of 200−500 mg of $V_2F_6{\cdot}4H_2O$[21] or a mixture of 60 wt % $VF_2{\cdot}4H_2O$ and 40 wt % $VF_3{\cdot}3H_2O$ were placed in a small alumina boat inside the tube and heated under flowing reaction gas for 14−18 h at 588 K. After completion of the dwell, the furnace was swung open to allow fast heat dissipation. Simultaneously, the reaction gas was changed to 10 L h^{-1} of dry argon. The most important reaction parameters are the hydrogen and water contents of the gas atmosphere, controlling the oxygen activity. This is decisive for controlled oxidation of vanadium. Consequently, a careful optimization of the reaction conditions is vital to the success of this reaction. Otherwise, leftover fluorine, partial oxidation to vanadium dioxide, or reduction to corundum-type V_2O_3 can be observed. All obtained products were characterized by X-ray powder diffraction (Siemens D5000 with Cu Kα_1 radiation, λ = 154.06 pm). Selected samples were studied by in situ high-temperature XRD (STOE Stadi-P, graphite-heated furnace, samples in SiO_2-glass capillaries under dried argon)

Received: May 25, 2012
Published: July 16, 2012

   dx.doi.org/10.1021/ic301096d | *Inorg. Chem.* 2012, 51, 8524−8529

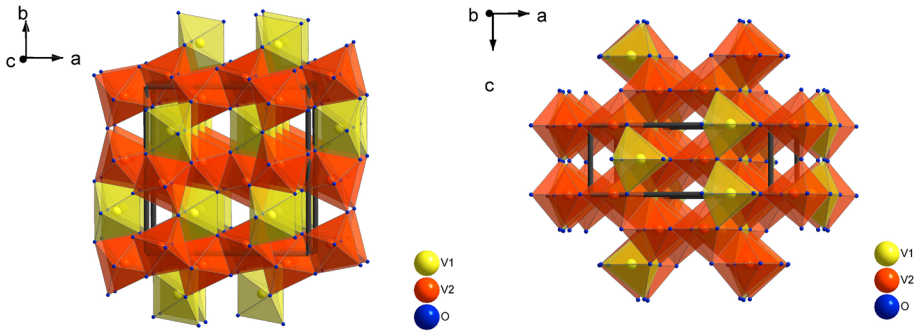

Figure 1. Unit cell of anosovite-type V_3O_5 with the connectivities of the two different coordination polyhedra, (a) showing the characteristic rows consisting of $(V1)O_6$ and $(V2)O_6$ octahedra, view along $[00\bar{1}]$. (b) Unit cell of anosovite-type V_3O_5, showing the edge-shared $(V2)O_6$ layers, view along $[0\bar{1}0]$.

with Mo Kα_1 radiation (λ = 70.93 pm). The program package FullProf October 2011[22] was used for structural refinements. Peak profiles were fitted with a Pseudo-Voigt function. Quantitative analysis of the oxygen content was performed by the well-established hot gas extraction method (LECO TC300/EF300) with zirconia (25.8 wt % O) as standard. The accuracy is ≈2% of the presented oxygen content ($V_3O_{5\pm0.1}$). Qualitative fluorine and hydrogen analyses were carried out by energy-dispersive X-ray spectroscopy (EDX, Hitachi S-2700), wavelength-dispersive X-ray analysis (WDX, Cameca SAS), and elemental analysis (CHNS, ThermoFinnigan Flash EA 1112). No significant amounts of fluorine or hydrogen could be detected in the here presented sample. With respect to the detection limits of the methods and equipment used, it can be stated that the amount of hydrogen is below 0.1 wt % and that of fluorine below 0.5 wt %. Thermoanalytical (DTA/TG) analysis (Linseis L81 II) was carried out under synthetic air (Alphagaz 1, Air Liquide, 80 mL h^{-1}) as well as under 10 vol % hydrogen in argon (NOXAL4, Air Liquide, 80 mL h^{-1}).

X-ray absorption spectroscopy (XAS) measurements were performed at the V K edge (5.465 keV, Si 111) at the Hamburg Synchrotron Radiation Laboratory, HASYLAB. The materials were mixed with polyethylene (≈5 mg oxide and ≈90 mg wax) and pressed to a pellet (13 mm diameter) with a force of 0.5 tons. For XAS data analysis, background subtraction and normalization were carried out by fitting linear polynomials to the pre-edge and the post-edge region of the absorption spectra, respectively.[23] The pseudoradial distribution function FT($\chi(k)*k^3$) was calculated by Fourier transforming the k^3-weighted experimental $\chi(k)$ function (k ranges from 2.0 to 11 Å^{-1}), multiplied by a Bessel window, into the R space.

Physical Property Measurements. A total of 14.221 mg of the anosovite-type V_3O_5 sample was packed in kapton foil and attached to the sample holder rod of a VSM for measuring the magnetic properties in a Quantum Design Physical Property Measurement System in the temperature range of 3−305 K with magnetic flux densities up to 80 kOe.

Computational Details. Complementary periodic quantum-chemical calculations were used in order to study the low-temperature and high-temperature polymorphs and the new anosovite-type V_3O_5 theoretically within the framework of density-functional theory (DFT). On the one hand, the CRYSTAL09 program package[24] was employed to carry out calculations with localized Gaussian basis sets. DFT calculations were performed on the basis of the Perdew−Wang functional (PWGGA).[25] In order to provide better comparability with the PAW results, small core effective core potentials (SCECP) from the Cologne group[26,27] as well as large core potentials (LCECP) from the Cambridge Theory of Condensed Matter group[28] have been employed for vanadium and oxygen in structure relaxations. SCECP basis sets of double-ζ quality with one polarization shell for vanadium and oxygen have been taken from our previous work on V_2O_3 with the bixbyite structure,[20] while LCECP basis sets were optimized separately. In preliminary calculations, the influence of semicore states in the SCECP calculations was found to be negligible regarding structural and energetic properties of the studied V_3O_5 polymorphs. We performed spin-polarized structure relaxations as well as vibrational frequency calculations in order to obtain zero-point and thermal contributions to the Gibbs energy G. On the other hand, calculations with the plane-wave code VASP[29] using the generalized-gradient approximation (GGA) according to Perdew, Burke, and Ernzerhof (PBE)[30] and the projector-augmented-wave (PAW) method[31] were performed. By combination of the phonon frequencies with Bose−Einstein statistics, thermodynamic properties at finite temperature are easily accessible.[32] For this purpose, the quasiharmonic phonons for the plane-wave code were calculated with the program FROPHO.[33]

RESULTS AND DISCUSSION

We have succeeded in preparing a new polymorph of V_3O_5 (for technical details see the Experimental Section). The grayish-black product was structurally characterized using X-ray powder diffraction. The new phase crystallizes in the anosovite-type, which is known from the high-temperature polymorph of Ti_3O_5.[34] This crystal structure type can also be found for ternary compounds such as $(Mg,Fe)Ti_2O_5$,[35] where it is known as pseudobrookite-type. In the anosovite-type structure (space group *Bbmm*), the cations occupy two nonequivalent Wyckoff sites: V1 is located at position 4*c* and V2 at position 8*f*. The resulting two different types of distorted VO_6 octahedra share edges and corners to form complex connection patterns. The connections between the two types of VO_6 octahedra are depicted in Figure 1a and b. Along the *b* direction, the polyhedral connection leads to the formation of characteristic rows. Parallel to (010), the $(V2)O_6$ octahedra form layers by sharing six edges with other octahedra. Along *b*, these layers are connected by edge sharing with $(V1)O_6$ linkers.

The results of the Rietveld refinement are given in Figure 2 and Tables 1 and 2. For an improved understanding of the following discussion, the results of a Rietveld refinement of the recently reported compound $V_3O_{4.61}N_{0.27}$, which also crystallizes in the anosovite/pseudobrookite-type structure,[36] have been added as an inset to Figure 2. The new phase exhibits a very narrow stability range in terms of the V:O ratio. For lower hydrogen contents in the reaction gas, prolonged dwell, or lower reaction temperatures, the formation of VO_2(M), the well-known ambient temperature polymorph of vanadium dioxide,[8] is observed. For higher reaction temperatures or higher hydrogen contents in the reaction gas, formation of the well-known corundum-type V_2O_3 can be found. By comparing the determined density of anosovite-type V_3O_5 (Table 1) with that of thermodynamically stable monoclinic V_3O_5 (space group $P2/c$: δ = 4.72 g cm^{-3}),[19] one finds that the value of the

dx.doi.org/10.1021/ic301096d | Inorg. Chem. 2012, 51, 8524−8529

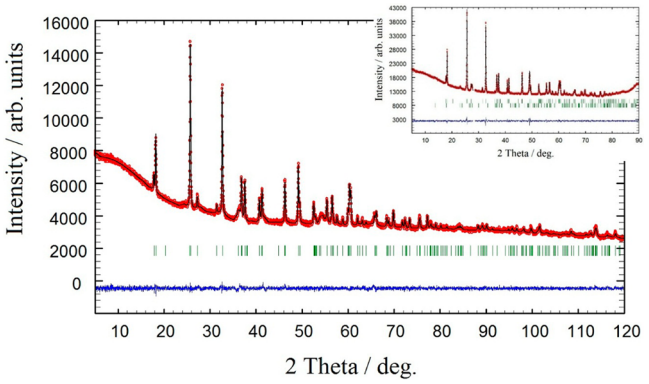

Figure 2. X-ray powder diffraction diagrams of anosovite-type V_3O_5 and $V_3O_{4.61}N_{0.27}$ (inset) with the results of the Rietveld refinements (λ = 154.06 pm).

Table 1. Results of the Rietveld Refinement

composition	V_3O_5
structure type	Anosovite
space group	*Bbmm* (No. 63)
lattice parameters	a = 971.87(4) pm
	b = 993.76(5) pm
	c = 370.02(2) pm
formula units	Z = 4
unit cell volume	V = 357.37(3) × 10^6 pm^3
calculated density	δ = 4.33 g/cm^3
diffractometer	Siemens D5000
wavelength	Cu Kα_1 (λ = 154.056 pm)
profile points	6144
2θ range	5−120°
R_{Bragg}	0.0535
R_{wp}	0.0174
R_{exp}	0.0157
S	1.11

Table 2. Refined Structural Parameters for Anosovite-Type V_3O_5[a]

atom	site	x	y	z	B_{iso} (Å^2)
V1	4*c*	0.8108(3)	1/4	0	0.12(9)
V2	8*f*	0.1343(2)	0.4389(2)	0	0.29(6)
O1	4*c*	0.238(1)	1/4	0	0.7
O2	8*f*	0.0477(8)	0.8835(7)	0	0.7
O3	8*f*	0.3172(8)	0.9293(8)	0	0.7

[a]Isotropic Debye-Waller factors for the oxygen atoms have been manually fixed to 0.7 Å^2.

anosovite-type polymorph is ≈8% smaller. Consequently, the orthorhombic phase cannot be prepared from the monoclinic polymorph by high-pressure methods.

The VO_6 octahedra together with the determined bond lengths are presented in Figure 3. The average vanadium−oxygen bond lengths of the (V1)O_6 octahedron (202.1 pm) and the (V2)O_6 octahedron (199.5 pm) are in pretty good agreement (identical within the error of refinements) with the determined bond lengths in $V_3O_{4.61}N_{0.27}$ (V1(O,N)$_6$: 201.3 pm. V2(O,N)$_6$: 199.5 pm). In order to study the effect of the vanadium oxidation state on the degree of distortion of the local octahedral environment, a Mulliken population analysis was performed using the LCAO PWxPW hybrid method. We used the unrestricted Kohn−Sham (UKS) approach. The V_6O_{10} unit cells contained 10 unpaired electrons corresponding to the formal charges 4+ (V1) and 3+ (V2). However, in the final wave function, we find only small differences between the spin populations on V1 (1.89) and V2 (1.61). These results do not support the classical expectation of formal V^{4+} and V^{3+} charge states but are in qualitative agreement with the experimentally observed small geometric differences between the two octahedral sites. For both V1 and V2 sites, similar Jahn−Teller distortions due to unpaired electrons on the vanadium atoms are found both in the XRD measurements and in the spin-unrestricted calculations. Thus, the two different oxidation states V^{3+}/V^{4+} do not clearly differentiate from the crystallographic sites, neither in the vanadium oxide nitride nor in the corresponding oxide. A similar behavior is also known from HT-Ti_3O_5.[37]

Examining the X-ray powder diffraction diagrams, it is obvious that the data of anosovite-type V_3O_5 exhibit a relatively high background compared to those of pseudobrookite-type $V_3O_{4.61}N_{0.27}$, especially in the 2 theta region between 5° and 15°. As known from chemical analyses, X-ray absorption spectroscopy, and also magnetic property measurements, $V_3O_{4.61}N_{0.27}$ shows no significant deviation from the average calculated valence of 3.34 for vanadium and, therefore, no significant deviation from the ideal stoichiometry. This behavior is mirrored from the good crystallinity of the compound and the low background in the diffraction diagram. The higher background found for anosovite-type V_3O_5, hence, is suggestive for the presence of significant amounts of amorphous species in the product. In fact, quantitative oxygen analysis of the sample resulted in 36.3 wt % oxygen, leading to a stoichiometry of $V_3O_{5.44}$ (expected for V_3O_5: 34.35 wt % oxygen).

In addition, in situ high temperature powder X-ray diffraction measurements in argon atmosphere show a reaction to VO_2(R) at ≈553 K (Figure 4), also indicating that the product contains considerable amounts of amorphous higher-valent vanadium oxides. For the oxide nitride $V_3O_{4.61}N_{0.27}$, in situ X-ray diffraction measurements showed a decomposition of the material, forming V_2O_3 and some amounts of monoclinic V_3O_5 and rutile-type VO_2(R). The average oxidation state of vanadium, respecting all these phases and their respective fraction, still shows a value close to 3.3. As it is very unlikely for the anosovite-type structure to incorporate major amounts of additional oxygen into the anion substructure,[36,38] the formation of vanadium dioxide at high temperatures in argon atmosphere is most simply explained by crystallization of the amorphous contents and/or reaction of the higher-valent species with V_3O_5.

In Figure 5, V K edge XANES spectra of anosovite-type V_3O_5, VO_2(B) and corundum-type V_2O_3 are compared. The pre-edge peak height of anosovite-type V_3O_5 is similar to that of VO_2(B), which indicates a significant amount of V^{4+} species in the material.[39] Figure 6 shows the FT($\chi(k)*k^3$) of anosovite-type V_3O_5. The pronounced amplitudes of V−V shells at distances above 2 Å indicate a well-defined medium-range order of the majority anosovite phase. This is corroborated by a good simulation of the experimental FT($\chi(k)*k^3$) of anosovite-type V_3O_5 on the basis of a corresponding model structure.

Further chemical analyses of the here-presented sample show neither significant amounts of incorporated hydrogen nor remaining fluorine (see Experimental Section for details). A fast oxidation of an anosovite-type V_3O_5 sample to pure V_2O_5 during thermogravimetric analysis under synthetic air starts at ≈443 K. Calculating the stoichiometry of the V_3O_5 sample

dx.doi.org/10.1021/ic301096d | *Inorg. Chem.* 2012, 51, 8524−8529

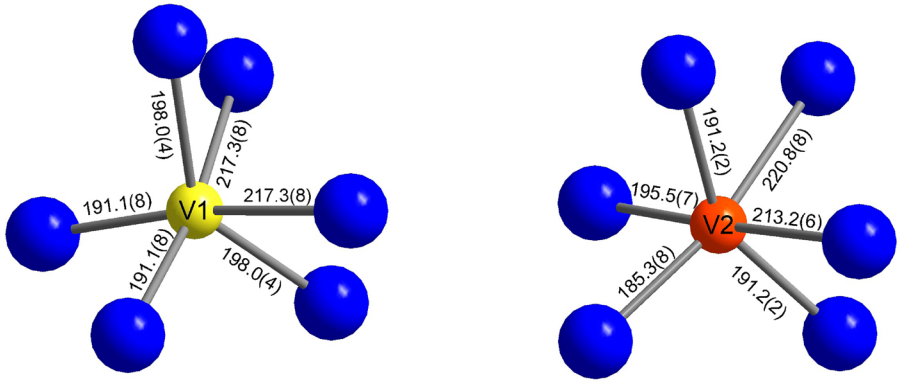

Figure 3. Coordination polyhedra and bond lengths (pm) in anosovite-type V_3O_5.

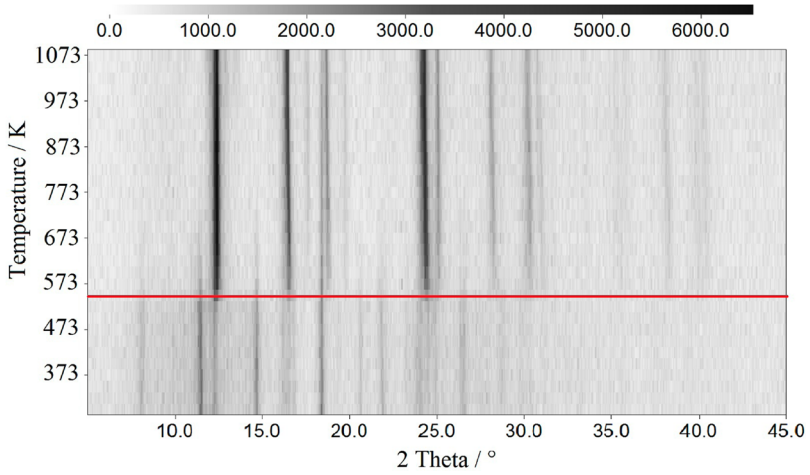

Figure 4. High temperature X-ray powder diffraction patterns of anosovite-type V_3O_5 in argon atmosphere (λ = 70.93 pm). At temperatures above ≈553 K (red line), the presence of VO_2(R) is observed. Gray scale reflects the intensity of the observed reflections.

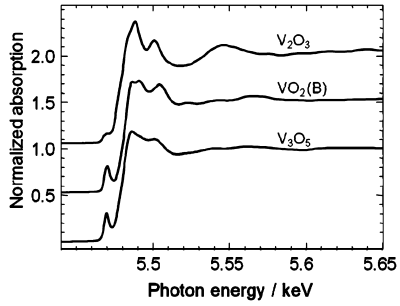

Figure 5. Vanadium K edge XANES spectra of anosovite-type V_3O_5, VO_2(B), and V_2O_3 with corundum structure.

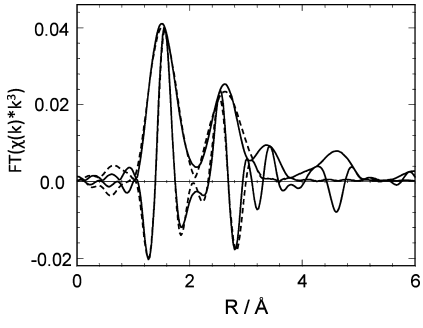

Figure 6. Vanadium K edge FT($\chi(k)$*k^3) (solid) of anosovite-type V_3O_5 together with a theoretical simulation (dotted).

resulted in a vanadium to oxygen ratio of about 1:2, and this gives an additional hint for a contamination of the material by oxygen-rich amorphous side products. This finding is supported by the observed weight change during thermogravimetric measurements under 10 vol % hydrogen in argon, resulting in reduction to single-phase corundum-type V_2O_3 and providing another indication of the starting material to be rather VO_2 than V_3O_5 in its overall stoichiometry. By taking all the facts into consideration, it is not surprising that the principally expected transformation of the orthorhombic to the monoclinic phase of V_3O_5 could not be observed in our DTA measurements. At ambient temperature an oxidation to vanadium dioxide is observed after six weeks, giving notice of the high reactivity of the material.

We also studied the relative stability of the two well-known V_3O_5 polymorphs and the new anosovite-type V_3O_5 theoretically at density-functional theory level. Corroborating the experimental findings, the low-temperature phase (space group *P*2/*c*) as well as the high-temperature phase (space group *I*2/*c*) are energetically favored compared to the anosovite-type polymorph for the complementary methods (depicted on the right side in Figure 7). The calculation employing the atom-centered basis set (CRYSTAL/PWGGA) yielded a 11 kJ/mol higher energy for the new orthorhombic polymorph and the plane-wave code (VASP/PBE) of about 15 kJ/mol. We find good agreement between calculated and measured structural parameters for anosovite-type V_3O_5 because the mean absolute

dx.doi.org/10.1021/ic301096d | *Inorg. Chem.* 2012, 51, 8524−8529

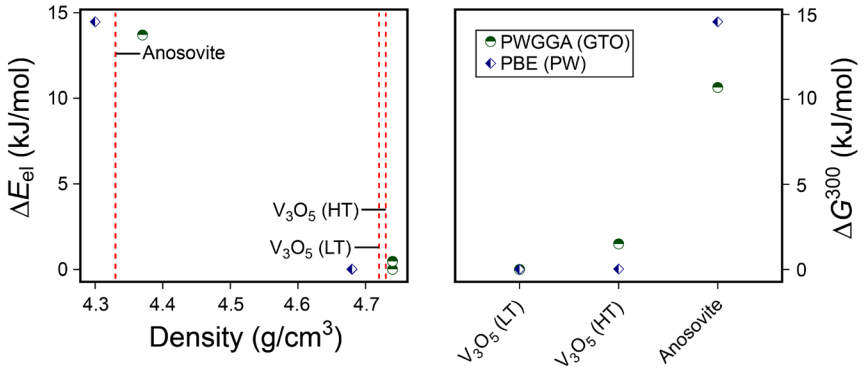

Figure 7. Left: Relative energy versus calculated density for the three polymorphs in comparison to the experimental values (red dashed lines); note that the low-temperature and high-temperature polymorphs yielded the same density and energy within the plane-wave calculation, but the space groups (LT: *P*2/*c* and HT: *I*2/*c*) remained. Right: Relative Gibbs energies at 300 K for the three polymorphs.

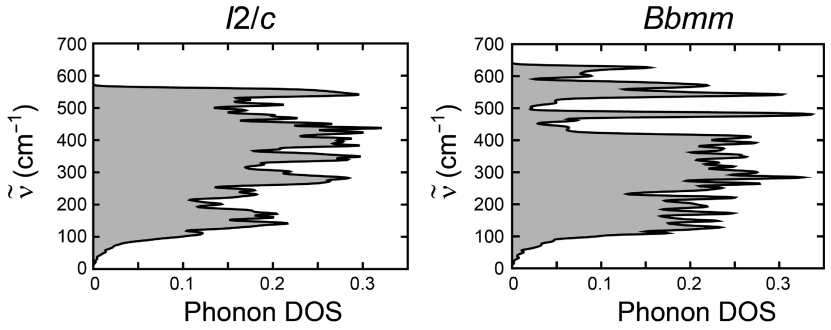

Figure 8. Phonon density of states of the high-temperature polymorph (*I*2/*c*) and the anosovite-type (*Bbmm*) V_3O_5.

percentage deviation with respect to the lattice parameters is 1.3% from CRYSTAL09/PWGGA and 1.2% from VASP/PBE. On the left side in Figure 7, the relative electronic energy is plotted versus the density with the literature values given as red dashed lines. In harmony with the experiment, the anosovite-type exhibits a smaller density compared to the low-temperature and high-temperature polymorph.

In order to analyze the dynamic stability, the phonon density of states (pDOS) was calculated for V_3O_5 with the high-temperature structure (*I*2/*c*) and the anosovite type (*Bbmm*). Only positive values are present in both pDOS in Figure 8. Imaginary values, which are usually displayed as negative, would indicate a structural instability. Thus, the new anosovite type is dynamically stable and located at a minimum of the potential energy surface. Consequently, V_3O_5 in the anosovite structure can be characterized as being metastable.

The temperature dependence of the magnetic ($\chi = M/H$) and the inverse magnetic susceptibility $\chi^{-1}(T)$ of the V_3O_5 sample are presented in Figure 9. The data were measured while warming the sample in a dc field of 10 kOe after zerofield cooling to the lowest available temperature. The susceptibility increases with decreasing temperature. The susceptibility data give no hint for magnetic ordering down to 3 K. Anosovite-type V_3O_5 exhibits Curie–Weiss behavior in the temperature range 60–300 K. The deviation from the Curie–Weiss law below 60 K is most likely due to the onset of magnetic correlations and/or crystal-field effects.

A least-squares fit of the susceptibility data in this temperature range resulted in an experimental magnetic moment of μ_{exp} = 1.86(1) μ_B/vanadium atom and a Weiss constant of θ_P = −47(1) K. The experimental magnetic moment is in between the values for free V^{3+} (2.83 μ_B) and V^{4+}

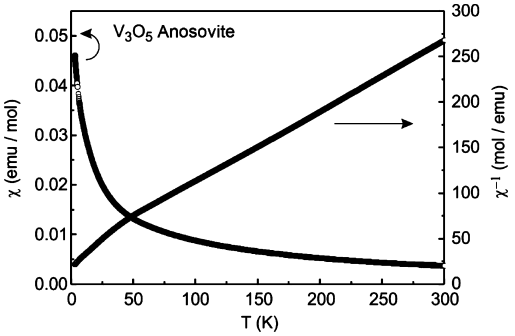

Figure 9. Temperature dependence of the magnetic and inverse magnetic susceptibility of the V_3O_5 sample measured at a flux density of 10 kOe.

(1.73 μ_B), assuming a spin-only high-spin state. In agreement with the XANES spectra the susceptibility data point to a considerable degree of tetravalent vanadium. This is similar to the recently reported compound $V_3O_{4.61}N_{0.27}$.[36] Nevertheless, one should keep in mind that the sample contamination by amorphous VO_2 also leads to a decrease in the experimental magnetic moment.

The magnetization isotherms at 10, 50, and 150 K are presented in Figure 10. At 50 and 150 K, we observe a linear increase in the magnetization with increasing field strength as expected for a paramagnetic material. The magnetization isotherm at 10 K shows a weak curvature, indicating the onset of field-induced parallel spin alignment.

dx.doi.org/10.1021/ic301096d | *Inorg. Chem.* 2012, 51, 8524–8529

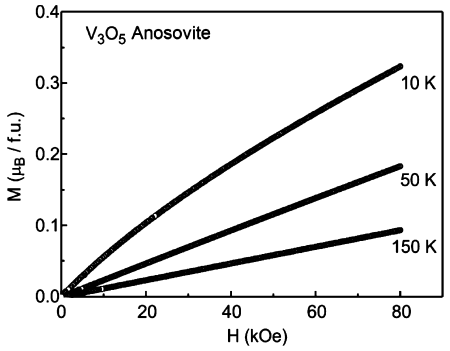

Figure 10. Magnetization isotherms of the V_3O_5 sample measured at 10, 50, and 150 K.

AUTHOR INFORMATION

Corresponding Author

*Fax: +49 (0) 30 314 79656. E-mail: lerch@chem.tu-berlin.de.

Notes

The authors declare no competing financial interest.

ACKNOWLEDGMENTS

Financial support from the Deutsche Forschungsgemeinschaft (SPP 1415) is gratefully acknowledged.

REFERENCES

(1) Haber, J. *Catal. Today* **2009**, *142*, 100−113.
(2) Hess, C. *ChemPhysChem* **2009**, *10*, 319−326.
(3) Liu, P.; Lee, S.-H.; Cheong, H. M.; Tracy, C. E.; Pitts, J. R.; Smith, R. D. *J. Electrochem. Soc.* **2002**, *149*, H76−H80.
(4) Prosini, P. P.; Xia, Y.; Fujieda, T.; Vellone, R.; Shikano, M.; Sakai, T. *Electrochim. Acta* **2001**, *46*, 2623−2629.
(5) Muster, J.; Kini, G. J.; Park, J. G.; Burghard, M. *Adv. Mater.* **2000**, *12*, 420−424.
(6) Magnéli, A.; Andersson, S.; Westman, S.; Kihlborg, L.; Holmberg, B.; Åsbrink, S.; Nordmark, C. In *Studies on the Crystal Chemistry of Titanium, Vanadium and Molybdenum Oxides at Elevated Temperatures, Final Technical Report 1*; DA-91-691-EUC-935; Stockholm. Univ. Inst. of Inorganic and Physical Chemistry, 1959; pp 23−30.
(7) Åsbrink, S.; Friberg, S.; Magnéli, A.; Andersson, G. *Acta Chem. Scand.* **1959**, *13*, 603.
(8) Andersson, G. *Acta Chem. Scand.* **1954**, *8*, 1599−1606.
(9) Horiuchi, H.; Tokonami, M.; Norimoto, N.; Nagasawa, H.; Bando, Y.; Takada, T. *Mater. Res. Bull.* **1971**, *6*, 833−843.
(10) Brückner, W.; Wich, G.; Terukov, E. I.; Chudnovskii, F. A. *Fiz. Tverd Tela (S.-Petersburg)* **1975**, *7*, 2191−2195.
(11) Åsbrink, S. *Mater. Res. Bull.* **1975**, *10*, 861−863.
(12) Terukov, E. I.; Chudnovski, F. A.; Reichelt, W.; Oppermann, H.; Brückner, W.; Brückner, H. P.; Moldenhauer, W. *Phys. Status Solidi* **1976**, *A37*, 541−546.
(13) Chudnovskii, F. A.; Terukov, E. I.; Khomskii, D. I. *Solid State Commun.* **1978**, *25*, 573−577.
(14) Okinaka, H.; Kosuge, K.; Kachi, S.; Takano, M.; Takada, T. *J. Phys. Soc. Jpn.* **1972**, *32*, 1148.
(15) Kachi, S.; Kosuge, K.; Okinaka, H. *J. Solid State Chem.* **1973**, *6*, 258−270.
(16) Åsbrink, S.; Hong, S. *Nature* **1979**, *279*, 624−625.
(17) Chudnovslii, F. A.; Terukov, E. I.; Khomskii, D. I. *Solid State Commun.* **1978**, *25*, 573−577.
(18) Terukov, E. I.; Chudnovskii, F. A. *Fiz. Tekh. Poluprovodn.* **1974**, *8*, 1226−1227.
(19) Åsbrink, S. *Acta Crystallogr., Sect.B* **1980**, *36*, 1332−1339.
(20) Weber, D.; Stork, A.; Nakhal, S.; Wessel, C.; Reimann, C.; Hermes, W.; Müller, A.; Ressler, T.; Pöttgen, R.; Bredow, T.; Dronskowski, R.; Lerch, M. *Inorg. Chem.* **2011**, *50*, 6762−6766.
(21) Nakhal, S.; Weber, D.; Irran, E.; Lerch, M.; Schwarz, B.; Ehrenberg, H. *Z. Anorg. Allg. Chem.* **2010**, *636* (11), 2061.
(22) Roisnel, T.; Rodriguez-Carvajal. *J. Mater. Sci. Forum* **2001**, *378*−*381*, 118−123.
(23) Ressler, T. J. *Synchrotron Radiat.* **1998**, *5*, 118−122.
(24) Dovesi, R.; Saunders, V. R.; Roetti, R.; Orlando, R.; Zicovich-Wilson, C. M.; Pascale, F.; Civalleri, B.; Doll, K.; Harrison, N. M.; Bush, I. J.; D'Arco, P.; Llunell, M. *CRYSTAL09 User's Manual*, University of Torino, Torino, 2009.
(25) Perdew, J. P.; Chevary, J. A.; Vosko, S. H.; Jackson, K. A.; Pederson, M. R.; Singh, D. J.; Fiolhais, C. *Phys. Rev. B* **1992**, *46*, 6671−6687.
(26) Burkatzki, M.; Filippi, C.; Dolg, M. *J. Chem. Phys.* **2007**, *126*, 234105−1−8.
(27) Burkatzki, M.; Filippi, C.; Dolg, M. *J. Chem. Phys.* **2008**, *129*, 164115−1−7.
(28) Trail, J. R.; Needs, R. J. *J. Chem. Phys.* **2005**, *122*, 174109−1−10. Trail, J. R.; Needs, R. J. *J. Chem. Phys.* **2005**, *122*, 014112−1−11. See also www.tcm.phy.cam.ac.uk/~mdt26/casino2_pseudopotentials.html.
(29) Kresse, G.; Furthmüller, J. *Comput. Mater. Sci.* **1996**, *6*, 15−50.
(30) Perdew, J. P.; Burke, K.; Ernzerhof, M. *Phys. Rev. Lett.* **1996**, *77*, 3865−3868.
(31) Blöchl, P. E. *Phys. Rev. B* **1994**, *50*, 17953−17979.
(32) Stoffel, R. P.; Wessel, C.; Lumey, M.-W.; Dronskowski, R. *Angew. Chem., Int. Ed.* **2010**, *49*, 5242−5266.
(33) Togo, A. F. RWTH Aachen University, 2007−2008. Available at http://fropho.sourceforge.net.
(34) Rusakov, A. A.; Zhdanov, G. S. *Dokl. Akad. Nauk SSSR* **1951**, *77*, 411−414.
(35) Teller, R. G.; Antonio, M. R.; Grau, A. E.; Gueguin, M; Kostiner, E. *J. Solid State Chem.* **1990**, *88*, 334−350.
(36) Nakhal, S.; Hermes, W.; Ressler, T.; Pöttgen, R.; Lerch, M. *Z. Anorg. Allg. Chem.* **2009**, *635*, 2016−2020.
(37) Onada, M. *J. Solid State Chem.* **1998**, *136*, 67−73.
(38) Grey, I. E.; Li, C.; Madsen, I. C. *J. Solid State Chem.* **1994**, *113*, 62−73.
(39) Wong, J.; Lytle, F. W.; Messmer, R. P.; Maylotte, D. H. *Phys. Rev. B.* **1984**, *30*, 5596−5610.

dx.doi.org/10.1021/ic301096d | *Inorg. Chem.* 2012, 51, 8524−8529